Journal of Computational Applied Mechanics 2021, 52(3): 366-393
DOI: 10.22059/jcamech.2021.306967.546

RESEARCH PAPER

Thermo-elastic creep analysis and life assessment of rotating thick pressurized cylindrical shells using third-order shear deformation theory

Tahereh Taghizadeh, Mohammad Zamani Nejad *

Department of Mechanical Engineering, Yasouj University, Yasouj, Iran

Abstract
Nowadays, In the present study, time-dependent thermo-elastic creep behavior and life assessment of rotating thick-walled cylindrical shells made of 304L austenitic stainless steel (304L SS) are investigated based on the third-order shear deformation theory (TSDT). Loading is composed of a uniform internal pressure, distributed temperature field, and a centrifugal body force due to rotating speed. Norton's law is utilized as the material creep constitutive model. Using the minimum total potential energy principle, a system of differential equations in terms of displacement and boundary conditions are derived. Then, the governing equations are solved with an analytical approach, which leads to an accurate solution. Subsequently, an iterative procedure is also proposed to determine the stresses and deformations at different creep times. Larson-Miller Parameter (LMP) and Robinson's linear life fraction damage rule are employed for assessing the creep damages and the remaining life of cylindrical shells. To the best of the researcher's knowledge, in the previous studies, there is no study carried out into third-order shear deformation theory for thermo-elastic creep analysis of cylinders. To validate the accuracy of the suggested method based on TSDT, a comparison among analytical results and those of the finite element method (FEM) is performed and very good agreement is found. The results indicate that the present analysis is accurate and computationally efficient.
Keywords: Creep, Life assessment, Rotating thick cylindrical shell, 304L austenitic stainless steel, Third-order shear deformation theory.

Introduction

Recently, the shells have attracted considerable attention from the research community due to high structural efficiency and wide applications in aerospace vehicles, aircraft industries, power generation, pressure vessels, nuclear reactors, petrochemical plants, submarines, buildings, and many other engineering applications [1-28]. In most of these applications, the shells are worked at high temperatures and under mechanical loading conditions. Due to long operational time, working in these situations lead to more thermo-mechanical stresses. Therefore, creep can impose the irreversible damages to structures and the creep analysis of these structures is a crucial necessity in the study of the above-mentioned applications. Failures of these components are always catastrophic, then, it is very important to the assessment of life in these structures. As a result, the creep behavior in these structures should be considered to stress analysis [29-37]. Choosing appropriate material of the structure is an important problem before performing the stress analysis. 304L austenitic stainless steel (304L SS) due to its excellent creep resistance has long creep life-time and can be utilized extensively in high-temperature applications [38]. For creep analysis, selecting the creep constitutive equations to model the creep behavior of the materials are needed and very important. It is worth noting that Norton's law is very popular because it is an easy and convenient model to use and the results obtained from this creep constitutive model are

* Corresponding author e-mail: m_zamani@yu.ac.ir; m.zamani.n@gmail.com

accurate and reasonable and it is one of the most important and widespread creep constitutive models to estimate the failure of structures [39-44]. Many researchers have worked on the creep analysis of components under thermo-elastic loadings which some of the relevant studies will be introduced [45-48]. Considering the presence of residual stress, Singh and Gupta [49] analyzed the problem of the steady-state creep response of a thick-walled cylinder made of functionally graded material (FGM) subjected to internal pressure via Hoffman's yield criterion. Nejad *et al*. [50] studied the steady-state creep behavior of rotating FGM thick-walled cylinders subjected to internal pressure, in which Norton's law was used to estimate material creep behavior. Using a semi-analytical approach, time-dependent creep analysis of FGM hollow cylinder operating under non-axisymmetric two-dimensional thermo-mechanical loadings was considered by Arefi and Loghman [51]. Moradi and Loghman [52] have used Bailey-Norton creep constitutive model to analyze the nonlinear creep response of a thick-walled cylinder made of stainless steel 316 under internal pressure and non-axisymmetric field by using a semi-analytical method.

In order to creep analysis, the classical theory of plane elasticity (PE) has been used in all the studies cited above, however, shear deformation theory (SDT) has not been considered for any of the mentioned solutions. During the last years, there have been numerous studies on the analysis of structures using SDT [53-63]. Shear deformation theory is a suitable theory to calculate stresses and displacements in axisymmetric thick shells. Although classical theory gives reasonable and acceptable results for thin shells, it is not an appropriate theory for thick shells [64, 65]. To take into account the effects of transverse shear deformations and rotary inertia, use of an appropriate shell theory like SDT in the thermo-elastic analysis of thick-walled shells for increasing the reliability of analysis becomes mandatory [66-73]. Stress analysis of thick cylindrical and conical shells made of homogeneous and functionally graded materials (FGMs) was studied extensively based on the SDT. Using the third-order shear deformation theory (TSDT), the stresses and displacements in the thick conical shell with variable thickness subjected to non-uniform internal pressure were investigated by Eipakchi [74]. Ghannad and Gharooni [75] carried out an elastic analysis of FG thick hollow cylindrical shells under internal and external pressure by applying an analytical approach based on the TSDT. Using the TSDT and analytical approach, Gharooni *et al*.[76] studied the thermo-elastic analysis of FGM thick cylindrical shells under internal pressure and thermal loading. Jabbari *et al*.[77] have used a semi-analytical approach based on the first-order shear deformation theory (FSDT) to analyze the thermo-elastic analysis of rotating thick truncated conical shells with variable thickness operating under internal and external pressures. Based on the FSDT, Kashkoli *et al*. [78, 79] proposed a semi-analytical method to investigate thermo-elastic creep stresses for life assessment of thick cylindrical and truncated conical shells made of 304 L austenitic stainless steel subjected to internal pressure. In other researches, Kashkoli *et al*.[80, 81] performed thermo-mechanical creep response of thick cylinders made of functionally graded material with constant and variable thicknesses under internal pressure using FSDT. Studies showed that the FSDT is acceptable theory to determine the radial displacement, radial stress, and circumferential stress, but the axial and von Mises stresses and axial displacement resulted from FSDT are considerably different than those from TSDT and FEM solution. Thus, FSDT is not very suitable and to overcome the above inconsistencies, an increase in the order of shear deformation theory is necessary. To the best of the author's knowledge, there have been no works that investigate the creep response of cylindrical shells based on TSDT.

In this study, we focus on the thermo-elastic creep response of a rotating thick-walled cylinder made of 304L austenitic stainless steel subjected to internal pressure. The governing formulations are derived using the minimum total potential energy principle based on the

TSDT. An analytical technique and iterative method are employed to solve the resulting equations and determine the stresses at different creep times. Robinson's linear life fraction damage rule is employed to obtain the creep damages and LMP is proposed to estimate the creep life of the cylinder. present research aim is to investigate the creep response of a rotating thick-walled cylinder by using accurate theory and simple analytical method. The results of the present study are also compared with those of FEM and there will be a good agreement between the results of the present study based on the TSDT and FEM results. The results confirm that the analytical method based on TSDT gives the most accurate results for radial and axial displacements, radial, circumferential and axial stresses.

Problem formulation

Thermo-elastic analysis

First, an analytical method was performed to obtain the thermal stresses of a thick cylindrical shell. A clamped-clamped thick-walled cylinder with an inner radius r_i, outer radius r_o, constant thickness h and length L is illustrated in Fig. 1. The cylinder is subjected to an inertia body force due to rotation of the cylinder with a constant angular speed and uniform internal pressure, and temperature field.

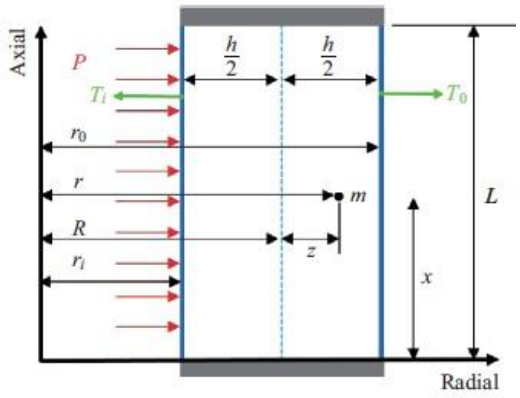

Figure 1. Cross section of the thick cylinder with clamped-clamped ends.

As Fig. 1 indicates, the location of a typical point m can be determined using the following equation:

$$\begin{cases} r = R + z \ , \ \left|\dfrac{z}{R}\right| < 1 \\ 0 \le x \le L \end{cases} \tag{1}$$

where R, z, r and x are the middle surface radius, thickness variable, the radius, and the vertical coordinate, respectively. The inner and outer radius of the cylinder is also written as:

$$\begin{cases} r_i = R - \dfrac{h}{2} = const. \\ r_o = R + \dfrac{h}{2} = const. \end{cases} \tag{2}$$

The displacement field is assumed as a polynomial of a variable z through the thickness based on the shear deformation theory. The approximate solution will be improved as the

number of terms in the polynomial function increase. In this study, for the displacement field, the third-order approximation is used. The general axisymmetric displacement field could be expressed as follows:

$$\begin{Bmatrix} U_x \\ U_z \end{Bmatrix} = \sum_{t=0}^{3} \begin{Bmatrix} u_t(x) \\ w_t(x) \end{Bmatrix} z^t \rightarrow \begin{cases} U_x(x,z) = u_0(x) + zu_1(x) + z^2u_2(x) + z^3u_3(x) \\ U_\theta(x,z) = 0 \\ U_z(x,z) = w_0(x) + zw_1(x) + z^2w_2(x) + z^3w_3(x) \end{cases} \tag{3}$$

in which U_x, U_θ and U_z are axial, circumferential, and radial displacement components respectively. u_t and w_t are unknown functions to determine the displacement field. The linear relations between the strain and the displacement components in the cylindrical coordinate system based on kinetic relations are expressed as:

$$\begin{cases} \varepsilon_x = \dfrac{\partial U_x}{\partial x} = \dfrac{du_0}{dx} + z\dfrac{du_1}{dx} + z^2\dfrac{du_2}{dx} + z^3\dfrac{du_3}{dx} \\ \varepsilon_\theta = \dfrac{U_z}{r} = \dfrac{1}{R+z}\left(w_0 + zw_1 + z^2w_2 + z^3w_3\right) \\ \varepsilon_z = \dfrac{\partial U_z}{\partial z} = w_1 + 2w_2z + 3w_3z^2 \\ \gamma_{xz} = \dfrac{\partial U_x}{\partial z} + \dfrac{\partial U_z}{\partial x} = \left(u_1 + \dfrac{dw_0}{dx}\right) + \left(2u_2 + \dfrac{dw_1}{dx}\right)z + \left(3u_3 + \dfrac{dw_2}{dx}\right)z^2 + z^3\dfrac{dw_3}{dx} \end{cases} \tag{4}$$

According to the linear constitutive thermos-elastic equations, the thermal stresses of homogenous and isotropic materials for an axisymmetric condition are also written as:

$$\begin{cases} \begin{Bmatrix} \sigma_x \\ \sigma_\theta \\ \sigma_z \end{Bmatrix} = \lambda E \begin{bmatrix} 1-\nu & \nu & \nu \\ \nu & 1-\nu & \nu \\ \nu & \nu & 1-\nu \end{bmatrix} \begin{Bmatrix} \varepsilon_x - \varepsilon_x^c \\ \varepsilon_\theta - \varepsilon_\theta^c \\ \varepsilon_z - \varepsilon_z^c \end{Bmatrix} - \lambda E(1+\nu)\alpha T \begin{bmatrix} 1 \\ 1 \\ 1 \end{bmatrix} \\ \tau_{xz} = \lambda E\left(\dfrac{1-2\nu}{2}\right)\gamma_{xz} \quad , \quad \lambda = \dfrac{1}{(1+\nu)(1-2\nu)} \end{cases} \tag{5}$$

Here E, ν and α are the modulus of elasticity, Poisson's ratio, and thermal expansion coefficient, σ_i, ε_i and ε_i^c represent the stresses, strains, and creep strains in the axial (x), circumferential (θ), and radial (z) directions, τ_{xz} and γ_{xz} are the shear stress and shear strain and T is the temperature distribution, respectively. The stress resultants are expressed as follows:

$$\begin{Bmatrix} N_x^{(i)} \\ N_\theta^{(i)} \\ N_z^{(i)} \\ N_{xz}^{(i)} \end{Bmatrix} = \int_{-h/2}^{h/2} \begin{Bmatrix} \sigma_x(R+z) \\ R\sigma_\theta \\ \sigma_z(R+z) \\ \tau_{xz}(R+z) \end{Bmatrix} \left(z^i/R\right) dz \qquad i = 0,1,2,3 \tag{6}$$

In this study, the minimum total potential energy principle can be employed to derive the governing equations and boundary conditions as:

$$\delta U = \delta W \tag{7}$$

where U and W represent the total strain energy and the total virtual work, respectively.

The strain energy of the elastic body and the external work are given by:

$$\begin{cases} U = \iiint_V U^* dV \\ dV = r dr d\theta dx = (R+z)\, dx d\theta dz \\ U^* = \dfrac{1}{2}\left(\sigma_x \varepsilon_x + \sigma_\theta \varepsilon_\theta + \sigma_z \varepsilon_z + \tau_{xz}\gamma_{xz}\right) \end{cases} \tag{8}$$

$$\begin{cases} W = \iint_s \left(\vec{f}_{sf}.\vec{u}\right) dS + \iiint_V \left(\vec{f}_{bf}.\vec{u}\right) dV \\ dS = r_i d\theta dx = \left(R - \dfrac{h}{2}\right) d\theta dx \\ \vec{f}_{sf}.\vec{u} = PU_z \\ \vec{f}_{bf}.\vec{u} = \rho\omega^2 (R+z) U_z \end{cases} \tag{9}$$

where ρ is density and ω is angular speed, which is assumed to be constant. Body force $\vec{f}_{bf}$ due to rotation of the cylinder and surface force $\vec{f}_{sf}$ due to internal pressure have been assumed. The variation of the strain energy becomes:

$$\delta U = \int_0^{2\pi}\int_0^{L}\int_{-h/2}^{h/2} \delta U^* (R+z)\, dz dx d\theta \tag{10}$$

Thus:

$$\frac{\delta U}{2\pi} = \int_0^{L}\int_{-h/2}^{h/2} \left(\sigma_x \delta\varepsilon_x + \sigma_\theta \delta\varepsilon_\theta + \sigma_z \delta\varepsilon_z + \tau_{xz}\delta\gamma_{xz}\right)(R+z)\, dz dx \tag{11}$$

The variation of the virtual work will be:

$$\delta W = \int_0^{2\pi}\int_0^{L} P\delta U_z \left(R - \frac{h}{2}\right) dx d\theta + \int_0^{2\pi}\int_0^{L}\int_{-h/2}^{h/2} \rho\omega^2 (R+z)^2\, \delta U_z\, dz dx d\theta \tag{12}$$

And:

$$\begin{aligned} \frac{\delta W}{2\pi} = & \int_0^{L} P\left(\delta w_0 + z\delta w_1 + z^2\delta w_2 + z^3\delta w_3\right)\left(R - \frac{h}{2}\right) dx \\ & + \int_0^{L}\int_{-h/2}^{h/2} \rho\omega^2 (R+z)^2 \left(\delta w_0 + z\delta w_1 + z^2\delta w_2 + z^3\delta w_3\right) dz dx \end{aligned} \tag{13}$$

By Substituting Eqs. (4)–(6) into Eq. (7), integrating by parts, and then setting each of the coefficients of δu_i and δw_i equal to zero, we obtain the following equations:

$$\begin{cases} \dfrac{d}{dx}\left(RN_x^{(i)}\right)-iRN_{xz}^{(i-1)}=0 \quad i=0,1,2,3 \\ \dfrac{d}{dx}\left(RN_{xz}^{(i)}\right)-iRN_z^{(i-1)}-N_\theta^{(i)}=-P\left(R-\dfrac{h}{2}\right)\left(\dfrac{-h}{2}\right)^i-\int_{-h/2}^{h/2}\rho\omega^2\left(R+z\right)^2 z^i dz \end{cases} \tag{14}$$

In addition, the boundary conditions are as:

$$R\left[\sum_{i=0}^{3}N_x^{(i)}\delta u_i+\sum_{i=0}^{3}N_{xz}^{(i)}\delta w_i\right]_0^L=0 \tag{15}$$

It should be noted that Eq. (14) is a set of differential equations in terms of the forces and moments that theses equations are equilibrium governing equations based on the TSDT and Eq. (15) represents the boundary conditions at the two ends of the cylinder. In order to solve Eq. (14), forces, and moments need to be obtained in terms of the displacement components. Substituting the stress components of Eq. (5) into Eq. (6) and considering Eqs. (3)– (4), the stress resultants could be derived as follows:

$$\begin{cases} N_x^{(i)}=(1-\nu)\sum_{t=0}^{3}\dfrac{du_t}{dx}\mathrm{X}_{t+i}+\nu\sum_{t=1}^{3}tw_t\mathrm{X}_{t-1+i}+\dfrac{\nu}{R}\sum_{k=0}^{3}w_k\Upsilon_{k+i}-(1+\nu)\Lambda_{1,i}- \\ \qquad\int_{-h/2}^{h/2}\lambda E\left((1-\nu)\varepsilon_x^c+\nu\left(\varepsilon_\theta^c+\varepsilon_z^c\right)\right)z^i\left(1+z/R\right)dz \\ N_\theta^{(i)}=\nu\sum_{t=0}^{3}\dfrac{du_t}{dx}\Upsilon_{t+i}+\nu\sum_{t=1}^{3}tw_t\Upsilon_{t-1+i}+(1-\nu)\sum_{k=0}^{3}w_k\mathrm{Z}_{k+i}-(1+\nu)\Lambda_{0,i}- \\ \qquad\int_{-h/2}^{h/2}\lambda E\left(\nu\left(\varepsilon_x^c+\varepsilon_z^c\right)+(1-\nu)\varepsilon_\theta^c\right)z^i dz \\ N_z^{(i)}=\nu\sum_{t=0}^{3}\dfrac{du_t}{dx}\mathrm{X}_{t+i}+(1-\nu)\sum_{t=1}^{3}tw_t\mathrm{X}_{t-1+i}+\dfrac{\nu}{R}\sum_{k=0}^{3}w_k\Upsilon_{k+i}-(1+\nu)\Lambda_{1,i} \\ -\int_{-h/2}^{h/2}\lambda E\left(\nu\left(\varepsilon_x^c+\varepsilon_\theta^c\right)+(1-\nu)\varepsilon_z^c\right)\left(1+z/R\right)z^i\ dz \\ N_{xz}^{(i)}=\left(\dfrac{1-2\nu}{2}\right)\left(\sum_{t=1}^{3}tu_t\mathrm{X}_{t-1+i}+\sum_{t=0}^{3}\dfrac{dw_t}{dx}\mathrm{X}_{t+i}\right) \end{cases} \tag{16}$$

The coefficients X_j, Υ_j, Z_j and $\Lambda_{L,j}$ are given in Appendix A. Substituting the stress resultants of Eq. (16) into Eq. (14) leads to the following equilibrium equations as a function of displacement components in the matrix form as:

$$\begin{cases} [A_1]\dfrac{d^2}{dx^2}\{\bar{y}\}+[A_2]\dfrac{d}{dx}\{\bar{y}\}+[A_3]\{\bar{y}\}=\{\bar{F}\} \\ \{\bar{y}\}=\{u_0 \quad u_1 \quad u_2 \quad u_3 \quad w_0 \quad w_1 \quad w_2 \quad w_3\}^T \end{cases} \tag{17}$$

Eq. (17) is a set of eight linear non-homogeneous equations. Since matric $[A_3]$ is irreversible and it's reverse will be used for solving the governing differential equations, the first equation in the set of Eq. (14) is integrated as:

$$RN_x^{(0)} = C_0 \tag{18}$$

In Eq. (17), It can be observed that that u_0 does not exist, but $\frac{du_0}{dx}$ does. Thus, considering $\frac{du_0}{dx}$ as υ which is a new parameter, we have:

$$u_0 = \int \upsilon dx + C_{15} \tag{19}$$

Using the mentioned changes, Eq. (17) can be written as:

$$\begin{cases} [B_1]\frac{d^2}{dx^2}\{y\} + [B_2]\frac{d}{dx}\{y\} + [B_3]\{y\} = \{F\} \\ \{y\} = \{\upsilon \quad u_1 \quad u_2 \quad u_3 \quad w_0 \quad w_1 \quad w_2 \quad w_3\}^T \end{cases} \tag{20}$$

The coefficients matrices $[B_i]_{8\times 8}$, and force vector $\{F\}$ are given in Appendix A.

1.1.1. *Thermo-elastic solution*

In order to obtain the differential equations for thermo-elastic analysis, creep strains ε_x^c, ε_θ^c and ε_z^c are ignored. Hence, deleting the creep strains from Eq. (20), and defining the differential operator $P(D)$, the governing equations for thick cylinders are derived.

$$[P(D)]\{y\} = \{F\} \tag{21}$$

where:

$$\begin{cases} [P(D)] = [B_1]D^2 + [B_2]D + [B_3] \\ D^2 = \frac{d^2}{dx^2} \ , \ D = \frac{d}{dx} \end{cases} \tag{22}$$

It is noted that the total solution of Eq.(22) which contains the general solution for the homogeneous case $\{y\}_h$ and particular solution $\{y\}_p$ can be written as follows :

$$\{y\} = \{y\}_h + \{y\}_p \tag{23}$$

The general solution for the homogeneous case is also expressed as follows:

$$\begin{cases} [P(D)]\{y\}_h = 0 \\ \{y\}_h = \{V\}e^{mx} \end{cases} \tag{24}$$

Eq. (24) is substituted into Eq. (21):

$$\left[m^2[B_1] + m[B_2] + [B_3]\right]\{V\} = \{0\} \tag{25}$$

In order to obtain the eigenvalues of Eq. (25), it is necessary that the determinant of coefficients is considered zero as:

$$\left|m^2[B_1] + m[B_2] + [B_3]\right| = 0 \tag{26}$$

The result of the determinant above is a sixteen-order polynomial, which is a function of m, the solution of which is a sixteen eigenvalue m_i. The eigenvalues are eight pairs of the conjugated root where a pair of the roots is zero. To derive the eigenvectors associated with the obtained eigenvalues, the eigenvalues are substituted into Eq. (25). Therefore, the homogeneous solution could be written as follows:

$$\{y\}_h = \sum_{i=1}^{14} C_i \{V\}_i e^{m_i x} \tag{27}$$

The particular solution may be obtained as:

$$\{y\}_p = [B_3]^{-1} \{F\} \tag{28}$$

Therefore, the total solution is expressed as:

$$\{y\} = \sum_{i=1}^{14} C_i \{V\}_i e^{m_i x} + [B_3]^{-1} \{F\} \tag{29}$$

Suppose that two ends of the cylinder are clamped-clamped. Thus, the boundary conditions for the mentioned cylinder are:

$$\begin{cases} x=0 \;\rightarrow\; u_0 = u_1 = u_2 = u_3 = w_0 = w_1 = w_2 = w_3 = 0 \\ x=L \;\rightarrow\; u_0 = u_1 = u_2 = u_3 = w_0 = w_1 = w_2 = w_3 = 0 \end{cases} \tag{30}$$

Therefore:

$$\begin{Bmatrix} U_x(x,z) \\ U_z(x,z) \end{Bmatrix}_{x=0,L} = \begin{Bmatrix} 0 \\ 0 \end{Bmatrix} \tag{31}$$

Note that the problem consists of 16 unknown constants including C_0 (Eq. (18)), C_1 to C_{14} (Eq. (29)), and C_{15} (Eq. (19)). Imposing the boundary conditions 16 linear algebraic equations are obtained. Solving the linear algebraic equations, 16 unknown constants can be determined.

Heat conduction analysis

In this study, the one-dimensional heat conduction equation in the cylinder, because of the steady-state and the heat generation absence assumptions, is expressed as:

$$\frac{d}{dr}\left[Kr \frac{dT}{dr} \right] = 0 \tag{32}$$

$r = R + z$ is substituted into Eq. (32) as:

$$\frac{d}{dz}\left[K(R+z) \frac{dT}{dz} \right] = 0 \tag{33}$$

Here, K denotes the thermal conduction coefficient. The distributed temperature field is obtained by solving Eq. (33) as follows:

$$T = g_1 \int \frac{dz}{K(R+z)} + g_2 - T_{ref} \tag{34}$$

In which g_1 and g_2 are integration constants which are determined using boundary condition and T_{ref} is the reference temperature. By assuming $T_{ref}=T_0$, and applying the boundary conditions $T(r=r_i)=T_i$, and $T(r=r_o)=T_o$, we obtain the temperature gradient distribution as follows:

$$T=\left(T_o-T_i\right)\left[\frac{\ln\left(\frac{R+z}{R-h/2}\right)}{\ln\left(\frac{R+h/2}{R-h/2}\right)}-1\right] \tag{35}$$

Governing equations for creep

For a thick cylindrical shell with creep behavior, the relations between strain rates and the displacement rates can be written as [78, 79]:

$$\begin{cases}\varepsilon_x=\dfrac{\partial \dot{U}_x}{\partial x}=\dfrac{d\dot{u}_0}{dx}+z\dfrac{d\dot{u}_1}{dx}+z^2\dfrac{d\dot{u}_2}{dx}+z^3\dfrac{d\dot{u}_3}{dx}\\ \varepsilon_\theta=\dfrac{\dot{U}_z}{r}=\dfrac{1}{R+z}\left(\dot{w}_0+z\dot{w}_1+z^2\dot{w}_2+z^3\dot{w}_3\right)\\ \varepsilon_z=\dfrac{\partial \dot{U}_z}{\partial z}=\dot{w}_1+2\dot{w}_2z+3\dot{w}_3z^2\\ \gamma_{xz}=\dfrac{\partial \dot{U}_x}{\partial z}+\dfrac{\partial \dot{U}_z}{\partial x}=\dot{u}_1+2\dot{u}_2z+3\dot{u}_3z^2+\dfrac{d\dot{w}_0}{dx}+z\dfrac{d\dot{w}_1}{dx}+z^2\dfrac{d\dot{w}_2}{dx}+z^3\dfrac{d\dot{w}_3}{dx}\\ \quad=\left(\dot{u}_1+\dfrac{d\dot{w}_0}{dx}\right)+\left(2\dot{u}_2+\dfrac{d\dot{w}_1}{dx}\right)z+\left(3\dot{u}_3+\dfrac{d\dot{w}_2}{dx}\right)z^2+z^3\dfrac{d\dot{w}_3}{dx}\end{cases} \tag{36}$$

Note that $\dot{(\ )}=\dfrac{d(\ )}{dt}$. The linear stress rates-strain rates relations can be expressed as follows:

$$\begin{cases}\begin{Bmatrix}\dot{\sigma}_x\\ \dot{\sigma}_\theta\\ \dot{\sigma}_z\end{Bmatrix}=\lambda E\begin{bmatrix}1-\nu & \nu & \nu\\ \nu & 1-\nu & \nu\\ \nu & \nu & 1-\nu\end{bmatrix}\begin{Bmatrix}\dot{\varepsilon}_x-\dot{\varepsilon}_x^c\\ \dot{\varepsilon}_\theta-\dot{\varepsilon}_\theta^c\\ \dot{\varepsilon}_z-\dot{\varepsilon}_z^c\end{Bmatrix}\\ \dot{\tau}_{xz}=\lambda E\left(\dfrac{1-2\nu}{2}\right)\dot{\gamma}_{xz}\end{cases} \tag{37}$$

where $\dot{\sigma}_i$, $\dot{\varepsilon}_i$ and $\dot{\varepsilon}_i^c$ denote the stresses, strains, and creep strains rate in the axial (x), circumferential (θ), and radial (z) directions, also $\dot{\tau}_{xz}$ and $\dot{\gamma}_{xz}$ are the shear stress and shear strain rate, respectively. According to Norton's law:

$$\begin{Bmatrix} \dot{\varepsilon}_x^c \\ \dot{\varepsilon}_\theta^c \\ \dot{\varepsilon}_z^c \end{Bmatrix} = \frac{A\sigma_e^{(n-1)}}{2} \begin{bmatrix} 2 & -1 & -1 \\ -1 & 2 & -1 \\ -1 & -1 & 2 \end{bmatrix} \begin{Bmatrix} \sigma_x \\ \sigma_\theta \\ \sigma_z \end{Bmatrix} \tag{38}$$

where:

$$\sigma_e = \frac{1}{\sqrt{2}} \sqrt{(\sigma_x - \sigma_\theta)^2 + (\sigma_x - \sigma_z)^2 + (\sigma_z - \sigma_\theta)^2 + 6\tau_{xz}^2} \tag{39}$$

Here, A and n are material constants for creep, and σ_e is the effective stress. Finally, assuming the angular speed and the pressure to be constant respect to time, the following equations of equilibrium considering Eqs. (14), for the creep problem are obtained as:

$$\begin{cases} \dfrac{d}{dx}\left(R\dot{N}_x^{(i)}\right) - iR\dot{N}_{xz}^{(i-1)} = 0 \\ \dfrac{d}{dx}\left(R\dot{N}_{xz}^{(i)}\right) - iR\dot{N}_z^{(i-1)} - \dot{N}_\theta^{(i)} = 0 \qquad i = 0,1,2,3 \end{cases} \tag{40}$$

In which:

$$\begin{Bmatrix} \dot{N}_x^{(i)} \\ \dot{N}_\theta^{(i)} \\ \dot{N}_z^{(i)} \\ \dot{N}_{xz}^{(i)} \end{Bmatrix} = \int_{-h/2}^{h/2} \begin{Bmatrix} \dot{\sigma}_x (R+z) \\ R\dot{\sigma}_\theta \\ \dot{\sigma}_z (R+z) \\ \dot{\tau}_{xz} (R+z) \end{Bmatrix} \left(z^i / R\right) dz \qquad i = 0,1,2,3 \tag{41}$$

It should be noted the temperature field is steady and its derivative with respect to time is zero. Thus, Substituting Eqs. (37) into Eqs. (41) and then into Eqs. (40) leads to the following set of differential equations in terms of displacement rates:

$$\begin{cases} [A_1]\dfrac{d^2}{dx^2}\{\dot{\bar{y}}\} + [A_2]\dfrac{d}{dx}\{\dot{\bar{y}}\} + [A_3]\{\dot{\bar{y}}\} = \{\bar{F}_c\} \\ \{\dot{\bar{y}}\} = \{\dot{u}_0 \quad \dot{u}_1 \quad \dot{u}_2 \quad \dot{u}_3 \quad \dot{w}_0 \quad \dot{w}_1 \quad \dot{w}_2 \quad \dot{w}_3\}^T \end{cases} \tag{42}$$

Eq. (42) is a set of eight linear non-homogeneous equations. As stated earlier, since matric $[A_3]$ is irreversible and it's reverse will be used in the subsequent calculations, Thus, the first equation in the set of Eq. (40) is integrated as:

$$R\dot{N}_x^{(0)} = D_0 \tag{43}$$

In Eq. (42), It can be observed that that $\dot{u}_0$ does not exist, but $\dfrac{d\dot{u}_0}{dx}$ does. If $\dfrac{d\dot{u}_0}{dx}$ is defined as new parameter $\dot{\upsilon}$, then we have:

$$\dot{u}_0 = \int \dot{\upsilon} dx + D_{15} \tag{44}$$

Applying the mentioned changes gives a new set of differential equations and boundary conditions as follows:

$$\begin{cases} [B_1]\dfrac{d^2}{dx^2}\{\dot{y}\}+[B_2]\dfrac{d}{dx}\{\dot{y}\}+[B_3]\{\dot{y}\}=\{F_c\} \\ \{\dot{y}\}=\{\dot{\upsilon} \quad \dot{u}_1 \quad \dot{u}_2 \quad \dot{u}_3 \quad \dot{w}_0 \quad \dot{w}_1 \quad \dot{w}_2 \quad \dot{w}_3\}^T \end{cases} \tag{45}$$

The force vector $\{F_c\}_{8\times1}$ is listed in Appendix B.

Creep solution

The complete solution of Eq. (45) is given as:

$$\{\dot{y}\}=\sum_{i=1}^{14} D_i \{V\}_i e^{m_i x}+[B_3]^{-1}\{F_c\} \tag{46}$$

The boundary conditions are:

$$\begin{cases} x=0 \ \rightarrow \ \dot{u}_0=\dot{u}_1=\dot{u}_2=\dot{u}_3=\dot{w}_0=\dot{w}_1=\dot{w}_2=\dot{w}_3=0 \\ x=L \ \rightarrow \ \dot{u}_0=\dot{u}_1=\dot{u}_2=\dot{u}_3=\dot{w}_0=\dot{w}_1=\dot{w}_2=\dot{w}_3=0 \end{cases} \tag{47}$$

The creep problem consists of 16 unknown constants including D_0 (Eq. (43)), D_1 to D_{14} (Eq.(46)) , and D_{15} (Eq. (44)) which can be found from the boundary conditions. An iterative numerical method is employed to find a distribution of stresses. When the stress rates have been determined, the creep stresses at any time will be obtained iteratively as:

$$\begin{cases} \sigma_{ij}^{(i)}(r,t_i)=\sigma_{ij}^{(i-1)}(r,t_{i-1})+\dot{\sigma}_{ij}^{(i)}(r,t_i)dt^{(i)} \qquad i,\, j=x,\theta,z \\ t_i=\sum_{k=0}^{i} dt^{(k)} \end{cases} \tag{48}$$

The stresses at the time t_{i-1} will be employed to obtain $\dot{\sigma}_{ij}^{(i)}(r,t_i)$. When the time t_i is zero, the stress distributions in the thermo-elastic state are calculated.

Creep life assessment

Several models have been suggested for estimating the creep lifetime, including time-fraction rule, strain-fraction rule, the reference stress, and skeletal stress method, continuum damage model, etc. Each of which has its own strengths and limitations. Experimental approaches for assessing the creep lifetime of components are usually time-consuming, expensive, and not practical for routine industrial applications. Analytical and numerical methods are also time-consuming, expensive, and beyond the usual engineering tasks. Also, the results of these methods are not accurate because of the uncertainty involved with material data, loading conditions, and constitutive equations. Therefore, relatively simple damage accumulation rule is vital for the successful life assessment method that provides reasonable and conservative results based on the less than ideal input data. In the industry, the most common method to creep damage assessment under variable thermomechanical loading is Robinson's linear life-fraction rule [82-86]. In this method, the fracture under variable load and temperatures can be predicted adding the creep life fractions consumed at each condition until their sum reaches the value of unity. The calculation of accumulated creep damage is carried out at the end of each time increment $\Delta t^i=0$ using the following equation:

$$D_f^i=\sum_{i=1}^{n}\frac{\Delta t^i}{t_r^i} \tag{49}$$

Here, D_f^i is creep damage and t_r^i denotes the creep fracture time at $i-th$ time increment. Based on the rupture criteria, $D_f^i = 1$ is used as an approximate value of rupture. The Larson-Miller parameter is employed to obtain the time to rupture as [78]:

$$P_{L-M} = T.\left(C + log_{10}(t_r)\right) \tag{50}$$

where T is temperature in Kelvin and t_r denote rupture time in hours. C is a physical parameter which the value of 20 is used as accepted value of C for most engineering materials and steels. The use of LMP is easier than other approaches to approximate creep fracture data. The variation of LMP versus stress for the 304L SS is demonstrated in Fig. 2. It can be observed that the LMP will remain constant for any constant stress level the combination of rupture time and test temperature [87]. The remaining life at any point in the radial direction of the conical shell can be expressed as:

$$RL^i = \left(1 - D_f^i\right) t_r^i \tag{51}$$

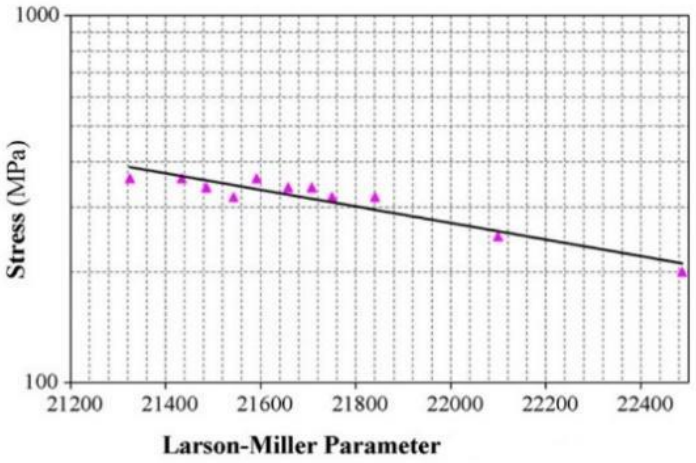

Figure 2. Variation of stress versus Larson–Miller parameter for the 304L SS [87].

Results and discussion

In this section, numerical results are computed for predicting creep behavior of thick cylindrical shell made of 304L austenitic stainless steel subjected to an internal pressure based on the TSDT. The cylindrical shell rotates and has clamped-clamped boundary conditions. 304L austenitic stainless steel referred to as 304L SS, is chosen as the material to use in high-temperature applications due to its excellent creep resistance capacity. Using the analytical method and programming the Maple software, the results are obtained. The following geometrical parameters and material properties for the cylindrical shell are considered [78, 79]:

$r_i = 40$ mm , $r_o = 60$ mm , $h = 20$ mm , $L = 1000$ mm

$E = 179$ GPa , $\nu = 0.3$, $\alpha = 16.9 \times 10^{-6}$ $1/^o\text{C}$, $K = 16.2$ $\text{W/m}^o\text{C}$

$\rho = 7900$ kg/m^3 , $A = 6.0121 \times 10^{-5}$ $\text{MPa}^{-n}\text{h}^{-1}$, $n = 5.7278$

Also, the values of the temperature boundary conditions, internal pressure, and angular velocity are assumed as follows:

$T_i = 625\ ^oC$, $T_o = 550\ ^oC$, $P = 60$ MPa , ω=500 rad/s

In order to show the accuracy and efficiency of the proposed solution based on the TSDT, the results of the analytical method are also validated and compared with the results which are obtained by the finite element method (FEM) model. Ansys is used to model a thick cylindrical shell in the FEM analysis. It is interesting to note that, when the number of elements in the FEM model is fine, results obtained from the analytical solution based on the TSDT are in good agreement with FEM results. A parametric study has been performed and the typical results are presented in a non-dimensional form in Figs.3-8.

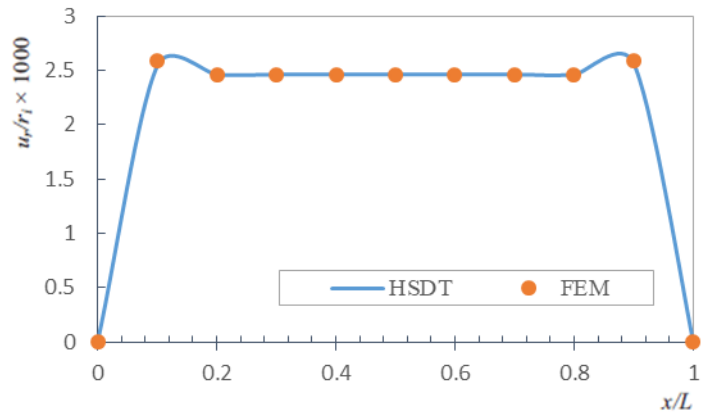

(a)

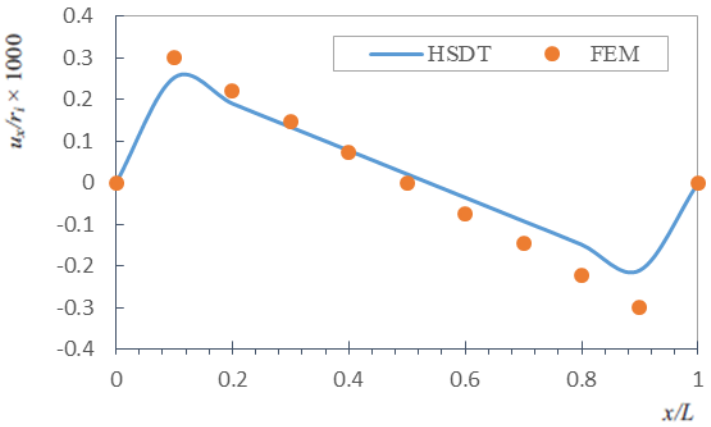

(b)

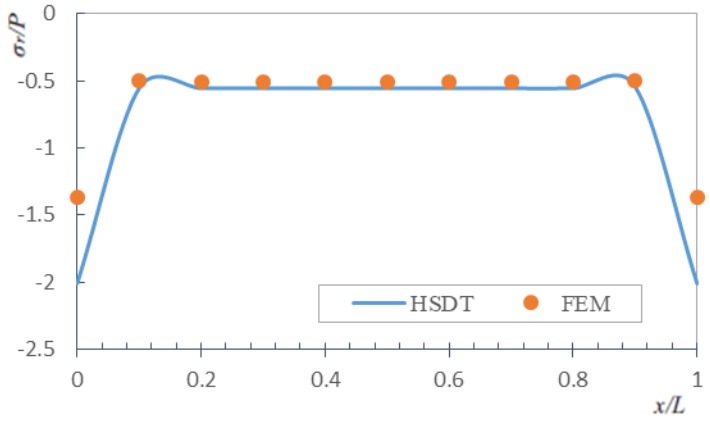

(c)

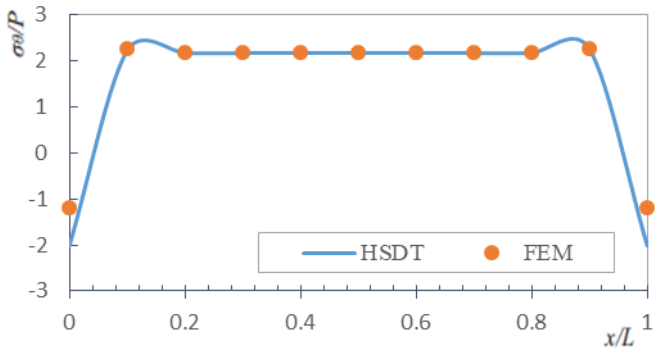

(d)

Figure 3. Variations of normalized creep displacements and stresses of the cylindrical shell across the dimensionless axial direction after 10000hr of creep process at the middle layer.

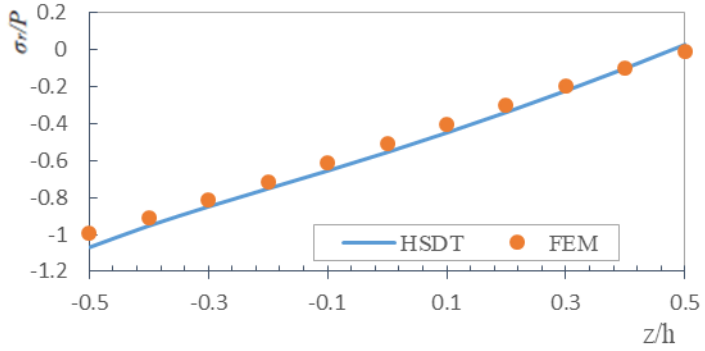

(a)

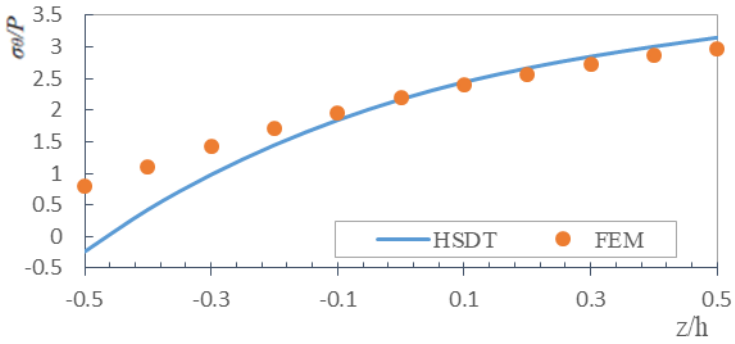

(b)

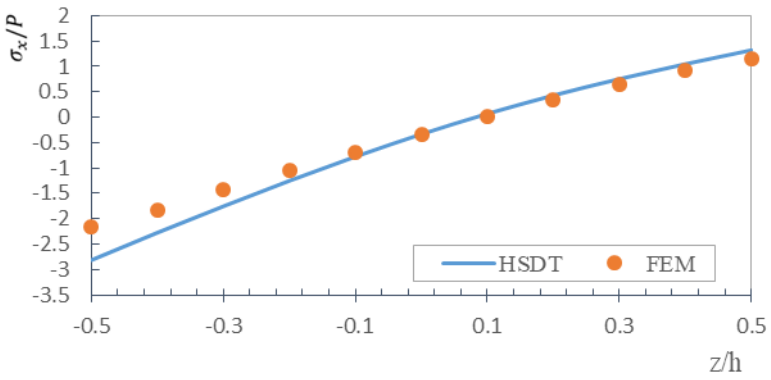

(c)

Figure 4. Variation of normalized stresses of the cylindrical shell across the dimensionless radial direction after 10000hr of creeping at $x = L/2$.

The creep displacements and stresses distributions at the middle layer of the thick cylinder after 10000hr of creeping for both FEM method and analytical solution based on TSDT are shown in Fig. 3. It can be seen that the results of the analytical approach agree very well with the FEM results. It is also found that the TSDT has an acceptable amount of accuracy when one wants to obtain radial displacement, axial displacements, radial stress, and circumferential stress. This means that TSDT for analyzing thick cylinder is accurate and computationally efficient. It is worthwhile to note that at points near the boundaries, the change in the creep displacements and stresses pattern is more considerable than that of the cylinder at points away from the boundaries. With these results, it can be observed that the absolute maximum of radial and axial displacements occurs at points near the boundaries.

Distributions of radial, circumferential, and axial stresses of the cylinder after 10000hr of creeping are demonstrated in Fig. 4. The same as Fig. 3, to demonstrate the validity of the present analysis, the results of analytical solution based on TSDT for creep stresses are compared with those obtained by FEM. According to Fig. 4, a very good agreement is found. It is evident from Figs. 4(a)-4(c) that, the absolute minimum of radial and axial stresses

occurs at the outer surface of the cylinder, while the absolute maximum of circumferential stress occurs at the outer surface.

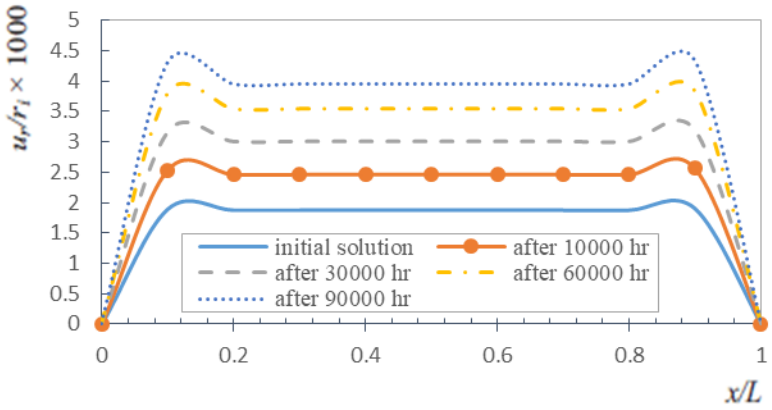

(a)

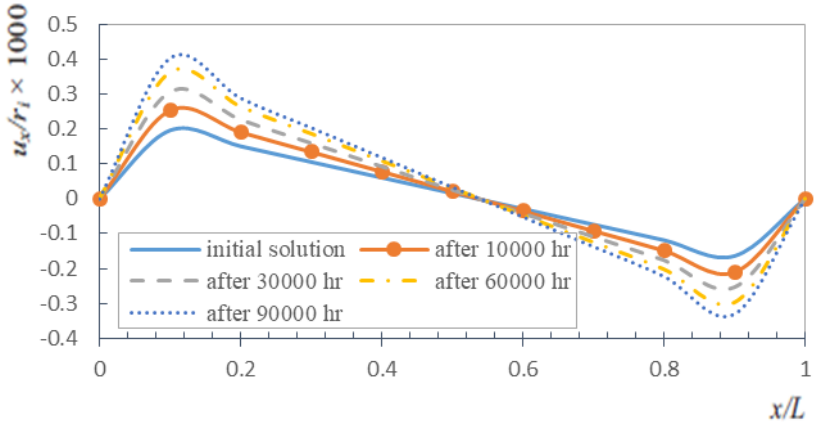

(b)

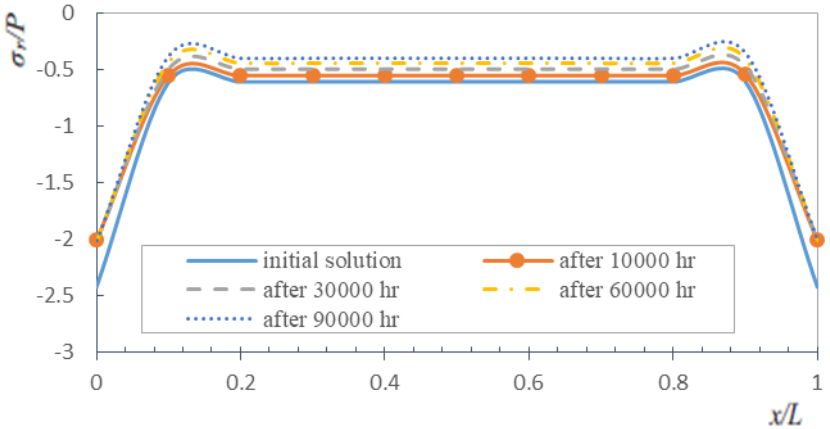

(c)

Figure 5. Variations of normalized radial and axial displacements and radial stress of the cylindrical shell across the dimensionless axial direction from initial solution at zero time up to 90000hr of creep process.

Effects of the creep time on the radial displacement, axial displacement and radial stress histories from the initial solution at zero time up to 90000hr of creep process with respect to

the ratio of x/L for middle layer of the cylindrical shell are demonstrated in Fig. 5. As shown in Figs. 5(a)-5(c), the absolute value of both radial and axial displacements is increased significantly with the increase of the creep time, while the absolute values of radial stress are decreased. It can also be observed that there is a considerable change in the radial displacement pattern with time during the creep process.

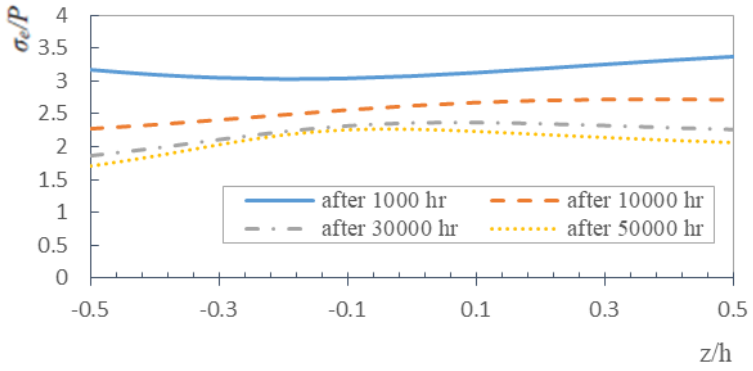

(a)

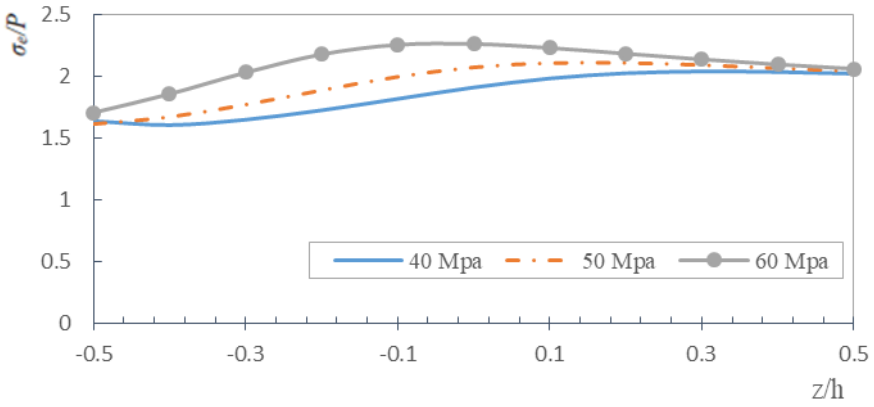

(b)

Figure 6. (a) Variation of normalized effective stress histories along the dimensionless radial direction (b) Effect of internal pressure on normalized effective stress after 50000 hr of creeping.

The effective stress histories up to 50000 hr and the effect of internal pressure on effective stress along the dimensionless radial direction are shown in Fig. 6. According to Fig. 6(a), The results reveal that the effective stresses at the outer surface of the cylinder are higher than those of the cylinder at the inner surface. It is also found that the effective stresses are decreased with the increase of the creep time. As Fig. 6(b) shows, the effective stresses are increased by increasing the internal pressure.

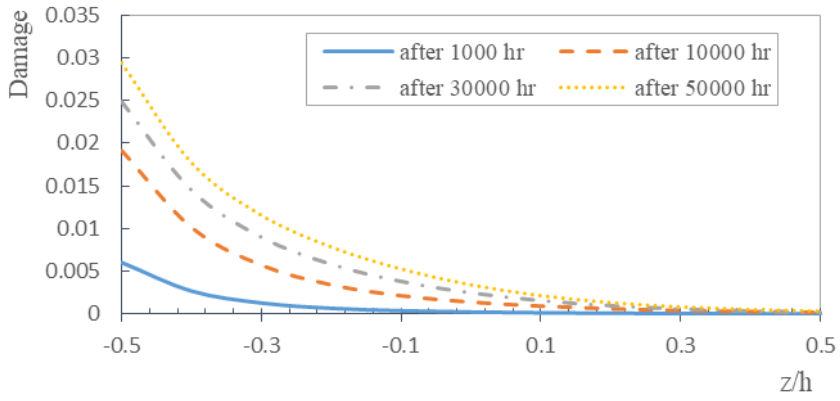

(a)

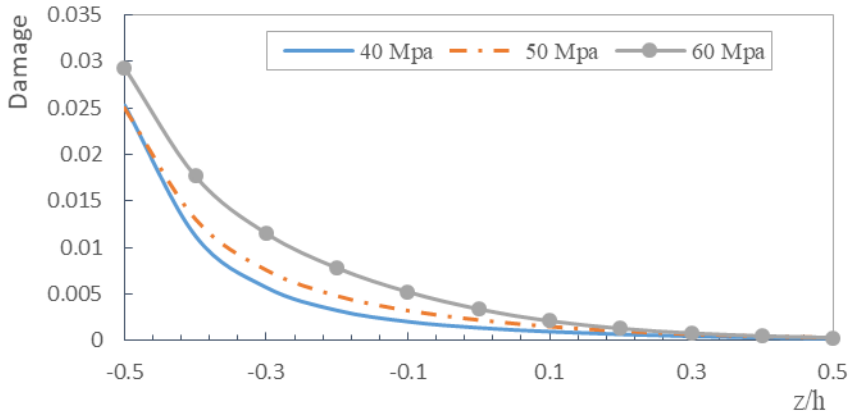

(b)

Figure 7. (a) Variation of creep damage along the dimensionless radial direction, (b) Effect of internal pressure on creep damage distribution after 50000 hr of creeping.

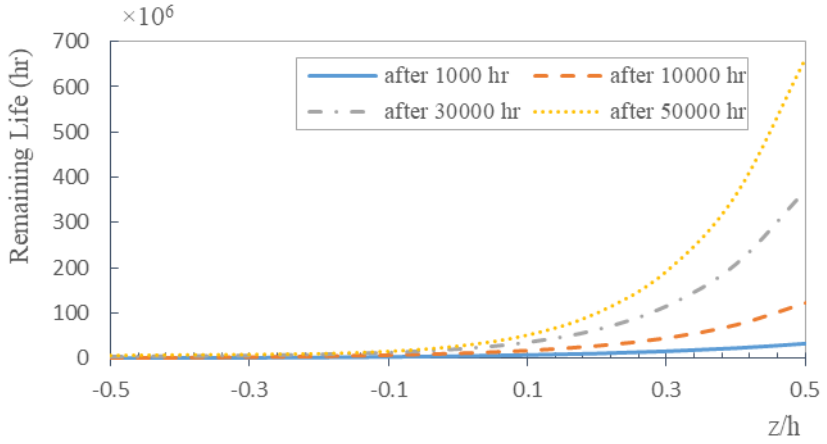

(a)

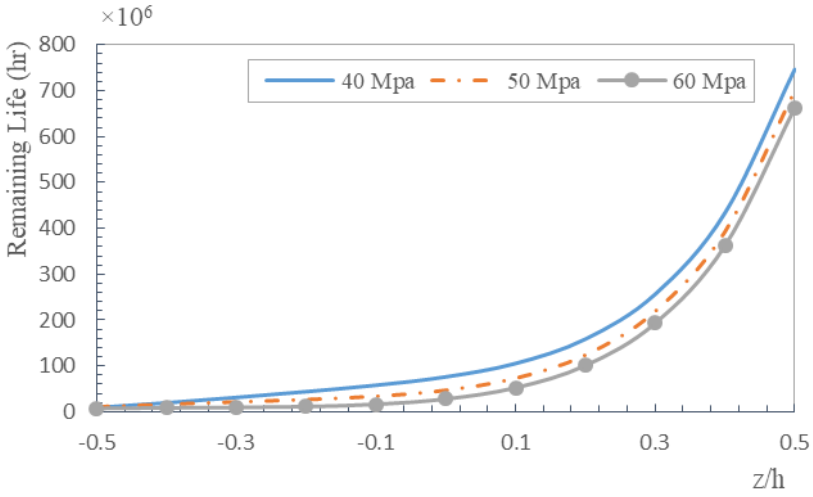

(b)

Figure 8. (a) Variation of remaining life along the dimensionless radial direction, (b) Effect of internal Pressure on remaining life distribution after 50000 hr of creeping.

The creep damage and the effect of internal pressure on the creep damage histories of the cylindrical shell with respect to z/h are illustrated in Fig. 7. Also, the remaining life and the internal pressure effect on the remaining life of the cylindrical shell across the dimensionless radial direction are shown in Fig. 8. As Figs. 7(a) and 8 (a) show, it is observed that maximum damages and the minimum remaining life occurs at the inner surface of the cylinder. Figures 7(b) and 8(b) present the effect of internal pressure on the creep damage and the remaining life of the cylindrical shell, respectively. It can be found that increasing the internal pressure has led to an increase in the creep damage and leads to reduce the remaining life as expected. Moreover, it is worth mentioning that there is a considerable change in creep damage and remaining life pattern at the inner surface and outer surface, respectively.

Conclusions

In this research, the time-dependent thermo-elastic creep response of a thick cylindrical shell made of 304 L SS subjected to the internal pressure and the thermal gradient was studied based on the TSDT. Norton's creep constitutive equation is used to model the creep behavior of the material. the governing set of differential equations are derived by applying the minimum total potential energy principle and these equations are solved using accurate and analytical method. Robinson's linear life fraction damage rule was used for obtaining the creep damage and the assessment of creep remaining life is determined using Larson-Miller parameter. To confirm the accuracy of the analytical solution based on TSDT, the results of the present work are also compared and validated with FEM results, and good agreement was found between the results. The remarkable obtained results in this investigation are as follows:

- The results indicate that the analytical approach based on the TSDT by increasing the order of shear deformation theory is a very appropriate theory in thick structural analysis to determine the radial and axial displacements and radial, circumferential and axial stresses with higher accuracy. It is worth noting that TSDT for analyzing a thick cylinder is accurate and computationally efficient.
- The results also confirm that at points near the boundaries, the change in the creep displacements and stresses pattern is more considerable than that of the cylinder at points away from the boundaries.

- It is noted that the absolute minimum of radial and axial stresses occurs at the outer surface of the cylinder, while the absolute maximum of circumferential stress occurs at the outer surface.
- The absolute value of both radial and axial displacements is increased with the increase of the creep time, while the absolute values of radial stress are decreased.
- It was concluded that the effective stresses are decreased as the creep time increases.
- The creep life becomes maximum at the minimum value of applied temperature in the outer surface.
- The creep damages at the inner surface of the cylindrical shell is serious.
- Furthermore, internal pressure has a great influence on the effective stresses, the creep damage, and the remaining life of the cylindrical shell. The effective stresses, as well as creep damages, increase by increasing internal pressure while an opposite behavior is experienced for the remaining life of cylinder and it decreased.

Appendix A

$$\begin{cases} \mathrm{X}_j = \int_{-h/2}^{h/2} \lambda E\left(1+z/R\right) z^j dz \\ \Upsilon_j = \int_{-h/2}^{h/2} \lambda E z^j dz \\ Z_j = \int_{-h/2}^{h/2} \lambda \dfrac{E}{R+z} z^j dz \\ \Lambda_{L,j} = \int_{-h/2}^{h/2} \lambda E \alpha_T T \left(1+z/R\right)^L z^j dz \qquad L=0,1 \qquad j=0,...,6 \end{cases} \tag{A1}$$

$$B_1 = \begin{bmatrix} [B_{11}]_{4\times4} & [B_{12}]_{4\times4} \\ [B_{13}]_{4\times4} & [B_{14}]_{4\times4} \end{bmatrix} \tag{A2}$$

$$[B_{11}] = \begin{bmatrix} 0 & 0 & 0 & 0 \\ 0 & R(1-\nu)X_2 & R(1-\nu)X_3 & R(1-\nu)X_4 \\ 0 & R(1-\nu)X_3 & R(1-\nu)X_4 & R(1-\nu)X_5 \\ 0 & R(1-\nu)X_4 & R(1-\nu)X_5 & R(1-\nu)X_6 \end{bmatrix} \tag{A3}$$

$$[B_{14}] = \frac{(1-2\nu)}{2} \begin{bmatrix} R\mathrm{X}_0 & R\mathrm{X}_1 & R\mathrm{X}_2 & R\mathrm{X}_3 \\ R\mathrm{X}_1 & RX_2 & RX_3 & RX_4 \\ R\mathrm{X}_2 & RX_3 & RX_4 & RX_5 \\ R\mathrm{X}_3 & RX_4 & RX_5 & RX_6 \end{bmatrix} \tag{A4}$$

$$[B_{12}] = [B_{13}] = [0]_{4\times4} \tag{A5}$$

$$B_2 = \begin{bmatrix} [B_{21}]_{4\times4} & [B_{22}]_{4\times4} \\ [B_{23}]_{4\times4} & [B_{24}]_{4\times4} \end{bmatrix} \tag{A6}$$

$$[B_{21}]=\begin{bmatrix} 0 & R(1-\nu)X_1 & R(1-\nu)X_2 & R(1-\nu)X_3 \\ R(1-\nu)X_1 & 0 & 0 & 0 \\ R(1-\nu)X_2 & 0 & 0 & 0 \\ R(1-\nu)X_3 & 0 & 0 & 0 \end{bmatrix} \tag{A7}$$

$$[B_{22}]=\begin{bmatrix} 0 & 0 & 0 & 0 \\ \frac{(2\nu-1)}{2}RX_0+\nu\Upsilon_1 & \frac{(4\nu-1)}{2}RX_1+\nu\Upsilon_2 & \frac{(6\nu-1)}{2}RX_2+\nu\Upsilon_3 & \frac{(8\nu-1)}{2}RX_3+\nu\Upsilon_4 \\ \frac{(4\nu-2)}{2}RX_1+\nu\Upsilon_2 & \frac{(6\nu-2)}{2}RX_2+\nu\Upsilon_3 & \frac{(8\nu-2)}{2}RX_3+\nu\Upsilon_4 & \frac{(10\nu-2)}{2}RX_4+\nu\Upsilon_5 \\ \frac{(6\nu-3)}{2}RX_2+\nu\Upsilon_3 & \frac{(8\nu-3)}{2}RX_3+\nu\Upsilon_4 & \frac{(10\nu-3)}{2}RX_4+\nu\Upsilon_5 & \frac{(12\nu-3)}{2}RX_5+\nu\Upsilon_6 \end{bmatrix} \tag{A8}$$

$$[B_{23}]=\begin{bmatrix} 0 & -\frac{(2\nu-1)}{2}RX_0-\nu\Upsilon_1 & -\frac{(4\nu-2)}{2}RX_1-\nu\Upsilon_2 & -\frac{(6\nu-3)}{2}RX_2-\nu\Upsilon_3 \\ 0 & -\frac{(4\nu-1)}{2}RX_1-\nu\Upsilon_2 & -\frac{(6\nu-2)}{2}RX_2-\nu\Upsilon_3 & -\frac{(8\nu-3)}{2}RX_3-\nu\Upsilon_4 \\ 0 & -\frac{(6\nu-1)}{2}RX_2-\nu\Upsilon_3 & -\frac{(8\nu-2)}{2}RX_3-\nu\Upsilon_4 & -\frac{(10\nu-3)}{2}RX_4-\nu\Upsilon_5 \\ 0 & -\frac{(8\nu-1)}{2}RX_3-\nu\Upsilon_4 & -\frac{(10\nu-2)}{2}RX_4-\nu\Upsilon_5 & -\frac{(12\nu-3)}{2}RX_5-\nu\Upsilon_6 \end{bmatrix} \tag{A9}$$

$$[B_{24}]=[0]_{4\times4} \tag{A10}$$

$$B_3=\begin{bmatrix} [B_{31}]_{4\times4} & [B_{32}]_{4\times4} \\ [B_{33}]_{4\times4} & [B_{34}]_{4\times4} \end{bmatrix} \tag{A11}$$

$$[B_{31}]=\begin{bmatrix} R(1-\nu)X_0 & 0 & 0 & 0 \\ 0 & -\frac{(1-2\nu)}{2}RX_0 & -2\frac{(1-2\nu)}{2}RX_1 & -3\frac{(1-2\nu)}{2}RX_2 \\ 0 & -2\frac{(1-2\nu)}{2}RX_1 & -4\frac{(1-2\nu)}{2}RX_2 & -6\frac{(1-2\nu)}{2}RX_3 \\ 0 & -3\frac{(1-2\nu)}{2}RX_2 & -6\frac{(1-2\nu)}{2}RX_3 & -9\frac{(1-2\nu)}{2}RX_4 \end{bmatrix} \tag{A12}$$

$$[B_{32}]=\begin{bmatrix} \nu\Upsilon_0 & \nu(RX_0+\Upsilon_1) & \nu(2RX_1+\Upsilon_2) & \nu(3RX_2+\Upsilon_3) \\ 0 & 0 & 0 & 0 \\ 0 & 0 & 0 & 0 \\ 0 & 0 & 0 & 0 \end{bmatrix} \tag{A13}$$

$$[B_{33}]=\begin{bmatrix} -\nu\Upsilon_0 & 0 & 0 & 0 \\ -\nu\left(\Upsilon_1+R\mathrm{X}_0\right) & 0 & 0 & 0 \\ -\nu\left(\Upsilon_2+2R\mathrm{X}_1\right) & 0 & 0 & 0 \\ -\nu\left(\Upsilon_3+3R\mathrm{X}_2\right) & 0 & 0 & 0 \end{bmatrix} \tag{A14}$$

$$[B_{34}]=\begin{bmatrix} -(1-\nu)\mathrm{Z}_0 & -(1-\nu)\mathrm{Z}_1-\nu\Upsilon_0 & -(1-\nu)\mathrm{Z}_2-2\nu\Upsilon_1 \\ -(1-\nu)\mathrm{Z}_1-\nu\Upsilon_0 & -(1-\nu)\left(\mathrm{Z}_2+R\mathrm{X}_0\right)-2\nu\Upsilon_1 & -(1-\nu)\left(\mathrm{Z}_3+2R\mathrm{X}_1\right)-3\nu\Upsilon_2 \\ -(1-\nu)\mathrm{Z}_2-2\nu\Upsilon_1 & -(1-\nu)\left(\mathrm{Z}_3+2R\mathrm{X}_1\right)-3\nu\Upsilon_2 & -(1-\nu)\left(\mathrm{Z}_4+4R\mathrm{X}_2\right)-4\nu\Upsilon_3 \\ -(1-\nu)\mathrm{Z}_3-3\nu\Upsilon_2 & -(1-\nu)\left(\mathrm{Z}_4+3R\mathrm{X}_2\right)-4\nu\Upsilon_3 & -(1-\nu)\left(\mathrm{Z}_5+6R\mathrm{X}_3\right)-5\nu\Upsilon_4 \end{bmatrix} \tag{A15}$$

$$\begin{bmatrix} -(1-\nu)\mathrm{Z}_3-3\nu\Upsilon_2 \\ -(1-\nu)\left(\mathrm{Z}_4+3R\mathrm{X}_2\right)-4\nu\Upsilon_3 \\ -(1-\nu)\left(\mathrm{Z}_5+6R\mathrm{X}_3\right)-5\nu\Upsilon_4 \\ -(1-\nu)\left(\mathrm{Z}_6+9R\mathrm{X}_4\right)-6\nu\Upsilon_5 \end{bmatrix}$$

$$\{F\}=\begin{Bmatrix} C_0+R(1+\nu)\Lambda_{1,0}+D_1^{(0)}(x) \\ R(1+\nu)\dfrac{d}{dx}\Lambda_{1,1}+\dfrac{d}{dx}D_1^{(1)}(x) \\ R(1+\nu)\dfrac{d}{dx}\Lambda_{1,2}+\dfrac{d}{dx}D_1^{(2)}(x) \\ R(1+\nu)\dfrac{d}{dx}\Lambda_{1,3}+\dfrac{d}{dx}D_1^{(3)}(x) \\ -(1+\nu)\Lambda_{0,0}-D_2^{(0)}(x)-P\left(R-\dfrac{h}{2}\right)-\rho\omega^2\left(R^2h+\dfrac{h^3}{12}\right) \\ -(1+\nu)\left(\Lambda_{0,1}+R\Lambda_{1,0}\right)-D_2^{(1)}(x)-D_3^{(0)}(x)+P\dfrac{h}{2}\left(R-\dfrac{h}{2}\right)-\rho\omega^2\dfrac{Rh^3}{6} \\ -(1+\nu)\left(\Lambda_{0,2}+2R\Lambda_{1,1}\right)-D_2^{(2)}(x)-2D_3^{(1)}(x)-P\dfrac{h^2}{4}\left(R-\dfrac{h}{2}\right)-\rho\omega^2\left(\dfrac{Rh^3}{12}+\dfrac{h^5}{80}\right) \\ -(1+\nu)\left(\Lambda_{0,3}+3R\Lambda_{1,2}\right)-D_2^{(3)}(x)-3D_3^{(2)}(x)+P\dfrac{h^3}{8}\left(R-\dfrac{h}{2}\right)-\rho\omega^2\left(\dfrac{Rh^5}{40}\right) \end{Bmatrix} \tag{A16}$$

$$
\begin{cases}
D_1^{(0)}(x) = R\int_{-h/2}^{h/2} \lambda E\left(\left(1-\nu\right)\varepsilon_x^c + \nu\left(\varepsilon_\theta^c + \varepsilon_z^c\right)\right)\left(1+z/R\right)\,dz \\
D_1^{(1)}(x) = R\int_{-h/2}^{h/2} \lambda E\left(\left(1-\nu\right)\varepsilon_x^c + \nu\left(\varepsilon_\theta^c + \varepsilon_z^c\right)\right) z\left(1+z/R\right)\,dz \\
D_1^{(2)}(x) = R\int_{-h/2}^{h/2} \lambda E\left(\left(1-\nu\right)\varepsilon_x^c + \nu\left(\varepsilon_\theta^c + \varepsilon_z^c\right)\right) z^2\left(1+z/R\right)\,dz \\
D_1^{(3)}(x) = R\int_{-h/2}^{h/2} \lambda E\left(\left(1-\nu\right)\varepsilon_x^c + \nu\left(\varepsilon_\theta^c + \varepsilon_z^c\right)\right) z^3\left(1+z/R\right)\,dz \\
D_2^{(0)}(x) = \int_{-h/2}^{h/2} \lambda E\left(\nu\left(\varepsilon_x^c + \varepsilon_z^c\right) + \left(1-\nu\right)\varepsilon_\theta^c\right)\,dz \\
D_2^{(1)}(x) = \int_{-h/2}^{h/2} \lambda E\left(\nu\left(\varepsilon_x^c + \varepsilon_z^c\right) + \left(1-\nu\right)\varepsilon_\theta^c\right)\,z dz \\
D_2^{(2)}(x) = \int_{-h/2}^{h/2} \lambda E\left(\nu\left(\varepsilon_x^c + \varepsilon_z^c\right) + \left(1-\nu\right)\varepsilon_\theta^c\right)\,z^2 dz \\
D_2^{(3)}(x) = \int_{-h/2}^{h/2} \lambda E\left(\nu\left(\varepsilon_x^c + \varepsilon_z^c\right) + \left(1-\nu\right)\varepsilon_\theta^c\right)\,z^3 dz \\
D_3^{(0)}(x) = R\int_{-h/2}^{h/2} \lambda E\left(\nu\left(\varepsilon_x^c + \varepsilon_\theta^c\right) + \left(1-\nu\right)\varepsilon_z^c\right)\left(1+z/R\right)\,dz \\
D_3^{(1)}(x) = R\int_{-h/2}^{h/2} \lambda E\left(\nu\left(\varepsilon_x^c + \varepsilon_\theta^c\right) + \left(1-\nu\right)\varepsilon_z^c\right)\left(1+z/R\right) z\ d \\
D_3^{(2)}(x) = R\int_{-h/2}^{h/2} \lambda E\left(\nu\left(\varepsilon_x^c + \varepsilon_\theta^c\right) + \left(1-\nu\right)\varepsilon_z^c\right)\left(1+z/R\right) z^2\ dz
\end{cases}
\tag{A17}
$$

Appendix B

$$
\left\{F_c\right\} = \begin{Bmatrix}
D_0 + E_1^{(0)}(x) \\
\frac{d}{dx}E_1^{(1)}(x) \\
\frac{d}{dx}E_1^{(2)}(x) \\
\frac{d}{dx}E_1^{(3)}(x) \\
-E_2^{(0)}(x) \\
-E_2^{(1)}(x) - E_3^{(0)}(x) \\
-E_2^{(2)}(x) - 2E_3^{(1)}(x) \\
-E_2^{(3)}(x) - 3E_3^{(2)}(x)
\end{Bmatrix}
\tag{B1}
$$

$$
\begin{cases}
E_1^{(0)}(x) = R\int\limits_{-h/2}^{h/2} \lambda E\left(\left(1-\upsilon\right)\dot{\varepsilon}_x^c + \upsilon\left(\dot{\varepsilon}_\theta^c + \dot{\varepsilon}_z^c\right)\right)\left(1+z/R\right)\,dz \\
E_1^{(1)}(x) = R\int\limits_{-h/2}^{h/2} \lambda E\left(\left(1-\upsilon\right)\dot{\varepsilon}_x^c + \upsilon\left(\dot{\varepsilon}_\theta^c + \dot{\varepsilon}_z^c\right)\right) z\left(1+z/R\right)\,dz \\
E_1^{(2)}(x) = R\int\limits_{-h/2}^{h/2} \lambda E\left(\left(1-\upsilon\right)\dot{\varepsilon}_x^c + \upsilon\left(\dot{\varepsilon}_\theta^c + \dot{\varepsilon}_z^c\right)\right) z^2\left(1+z/R\right)\,dz \\
E_1^{(3)}(x) = R\int\limits_{-h/2}^{h/2} \lambda E\left(\left(1-\upsilon\right)\dot{\varepsilon}_x^c + \upsilon\left(\dot{\varepsilon}_\theta^c + \dot{\varepsilon}_z^c\right)\right) z^3\left(1+z/R\right)\,dz \\
E_2^{(0)}(x) = \int\limits_{-h/2}^{h/2} \lambda E\left(\upsilon\left(\dot{\varepsilon}_x^c + \dot{\varepsilon}_z^c\right) + \left(1-\upsilon\right)\dot{\varepsilon}_\theta^c\right)\,dz \\
E_2^{(1)}(x) = \int\limits_{-h/2}^{h/2} \lambda E\left(\upsilon\left(\dot{\varepsilon}_x^c + \dot{\varepsilon}_z^c\right) + \left(1-\upsilon\right)\dot{\varepsilon}_\theta^c\right)\,z dz \\
E_2^{(2)}(x) = \int\limits_{-h/2}^{h/2} \lambda E\left(\upsilon\left(\dot{\varepsilon}_x^c + \dot{\varepsilon}_z^c\right) + \left(1-\upsilon\right)\dot{\varepsilon}_\theta^c\right)\,z^2 dz \\
E_2^{(3)}(x) = \int\limits_{-h/2}^{h/2} \lambda E\left(\upsilon\left(\dot{\varepsilon}_x^c + \dot{\varepsilon}_z^c\right) + \left(1-\upsilon\right)\dot{\varepsilon}_\theta^c\right)\,z^3 dz \\
E_3^{(0)}(x) = R\int\limits_{-h/2}^{h/2} \lambda E\left(\upsilon\left(\dot{\varepsilon}_x^c + \dot{\varepsilon}_\theta^c\right) + \left(1-\upsilon\right)\dot{\varepsilon}_z^c\right)\left(1+z/R\right)\,dz \\
E_3^{(1)}(x) = R\int\limits_{-h/2}^{h/2} \lambda E\left(\upsilon\left(\dot{\varepsilon}_x^c + \dot{\varepsilon}_\theta^c\right) + \left(1-\upsilon\right)\dot{\varepsilon}_z^c\right)\left(1+z/R\right) z dz \\
E_3^{(2)}(x) = R\int\limits_{-h/2}^{h/2} \lambda E\left(\upsilon\left(\dot{\varepsilon}_x^c + \dot{\varepsilon}_\theta^c\right) + \left(1-\upsilon\right)\dot{\varepsilon}_z^c\right)\left(1+z/R\right) z^2 dz
\end{cases}
\tag{B2}
$$

References

[1] M. Z. Nejad, G. Rahimi, M. Ghannad, Set of field equations for thick shell of revolution made of functionally graded materials in curvilinear coordinate system, *Mechanics*, Vol. 77, No. 3, pp. 18-26, 2009.

[2] P. Fatehi, M. Z. Nejad, Effects of material gradients on onset of yield in FGM rotating thick cylindrical shells, *International Journal of Applied Mechanics*, Vol. 6, No. 04, pp. 1450038, 2014.

[3] M. Z. Nejad, M. Jabbari, M. Ghannad, A semi-analytical solution of thick truncated cones using matched asymptotic method and disk form multilayers, *Archive of Mechanical Engineering*, Vol. 61, No. 3, 2014.

[4] M. Z. Nejad, P. Fatehi, Exact elasto-plastic analysis of rotating thick-walled cylindrical pressure vessels made of functionally graded materials, *International Journal of Engineering Science*, Vol. 86, pp. 26-43, 2015.

[5] R. Ghajar, M. Shokrieh, A. R. Shajari, Transient thermo-visco-elastic response of a functionally graded non-axisymmetric cylinder, *Journal of Computational Applied Mechanics*, Vol. 46, No. 2, pp. 191-204, 2015.

[6] Z. Mazarei, M. Z. Nejad, A. Hadi, Thermo-elasto-plastic analysis of thick-walled spherical pressure vessels made of functionally graded materials, *International Journal of Applied Mechanics*, Vol. 8, No. 04, pp. 1650054, 2016.

[7] M. Z. Nejad, M. Jabbari, M. Ghannad, A general disk form formulation for thermo-elastic analysis of functionally graded thick shells of revolution with arbitrary curvature and variable thickness, *Acta Mechanica*, Vol. 228, No. 1, pp. 215-231, 2017.

[8] M. Zamani Nejad, M. Jabbari, A. Hadi, A review of functionally graded thick cylindrical and conical shells, *Journal of Computational Applied Mechanics*, Vol. 48, No. 2, pp. 357-370, 2017.

[9] A. Afshin, M. Zamani Nejad, K. Dastani, Transient thermoelastic analysis of FGM rotating thick cylindrical pressure vessels under arbitrary boundary and initial conditions, *Journal of Computational Applied Mechanics*, Vol. 48, No. 1, pp. 15-26, 2017.

[10] M. Gharibi, M. Zamani Nejad, A. Hadi, Elastic analysis of functionally graded rotating thick cylindrical pressure vessels with exponentially-varying properties using power series method of Frobenius, *Journal of Computational Applied Mechanics*, Vol. 48, No. 1, pp. 89-98, 2017.

[11] R. Jamshidi, A. A. Jafari, Transverse sensing of simply supported truncated conical shells, *Journal of Computational Applied Mechanics*, Vol. 49, No. 2, pp. 212-230, 2018.

[12] F. Ahmadi, M. Hoseini, Parametric study of nonlinear buckling capacity of short cylinders with Hemispherical heads under hydrostatic pres-sure, *Journal of Computational Applied Mechanics*, 2020.

[13] M. Emadi, M. Z. Nejad, S. Ziaee, A. Hadi, Buckling analysis of arbitrary two-directional functionally graded nano-plate based on nonlocal elasticity theory using generalized differential quadrature method, *Steel and Composite Structures*, Vol. 39, No. 5, pp. 565-581, 2021.

[14] T. Ebrahimi, M. Z. Nejad, H. Jahankohan, A. Hadi, Thermoelastoplastic response of FGM linearly hardening rotating thick cylindrical pressure vessels, *Steel and Composite Structures*, Vol. 38, No. 2, pp. 189-211, 2021.

[15] M. M. Khoram, M. Hosseini, A. Hadi, M. Shishehsaz, Bending Analysis of Bidirectional FGM Timoshenko Nanobeam Subjected to Mechanical and Magnetic Forces and Resting on Winkler–Pasternak Foundation, *International Journal of Applied Mechanics*, Vol. 12, No. 08, pp. 2050093, 2020.

[16] E. Zarezadeh, V. Hosseini, A. Hadi, Torsional vibration of functionally graded nano-rod under magnetic field supported by a generalized torsional foundation based on nonlocal elasticity theory, *Mechanics Based Design of Structures and Machines*, Vol. 48, No. 4, pp. 480-495, 2020.

[17] A. Barati, M. M. Adeli, A. Hadi, Static torsion of bi-directional functionally graded microtube based on the couple stress theory under magnetic field, *International Journal of Applied Mechanics*, Vol. 12, No. 02, pp. 2050021, 2020.

[18] M. Najafzadeh, M. M. Adeli, E. Zarezadeh, A. Hadi, Torsional vibration of the porous nanotube with an arbitrary cross-section based on couple stress theory under magnetic field, *Mechanics Based Design of Structures and Machines*, pp. 1-15, 2020.

[19] A. Barati, A. Hadi, M. Z. Nejad, R. Noroozi, On vibration of bi-directional functionally graded nanobeams under magnetic field, *Mechanics Based Design of Structures and Machines*, pp. 1-18, 2020.

[20] K. Dehshahri, M. Z. Nejad, S. Ziaee, A. Niknejad, A. Hadi, Free vibrations analysis of arbitrary three-dimensionally FGM nanoplates, *Advances in nano research*, Vol. 8, No. 2, pp. 115-134, 2020.

[21] R. Noroozi, A. Barati, A. Kazemi, S. Norouzi, A. Hadi, Torsional vibration analysis of bi-directional FG nano-cone with arbitrary cross-section based on nonlocal strain gradient elasticity, *Advances in nano research*, Vol. 8, No. 1, pp. 13-24, 2020.

[22] M. Hosseini, M. Shishesaz, A. Hadi, Thermoelastic analysis of rotating functionally graded micro/nanodisks of variable thickness, *Thin-Walled Structures*, Vol. 134, pp. 508-523, 2019.

[23] M. Z. Nejad, N. Alamzadeh, A. Hadi, Thermoelastoplastic analysis of FGM rotating thick cylindrical pressure vessels in linear elastic-fully plastic condition, *Composites Part B: Engineering*, Vol. 154, pp. 410-422, 2018.

[24] A. Hadi, A. Rastgoo, N. Haghighipour, A. Bolhassani, Numerical modelling of a spheroid living cell membrane under hydrostatic pressure, *Journal of Statistical Mechanics: Theory and Experiment*, Vol. 2018, No. 8, pp. 083501, 2018.

[25] M. Z. Nejad, A. Hadi, A. Omidvari, A. Rastgoo, Bending analysis of bi-directional functionally graded Euler-Bernoulli nano-beams using integral form of Eringen's non-local elasticity theory, *Structural engineering and mechanics: An international journal*, Vol. 67, No. 4, pp. 417-425, 2018.

[26] A. Hadi, M. Z. Nejad, M. Hosseini, Vibrations of three-dimensionally graded nanobeams, *International Journal of Engineering Science*, Vol. 128, pp. 12-23, 2018.

[27] A. Soleimani, K. Dastani, A. Hadi, M. H. Naei, Effect of out-of-plane defects on the postbuckling behavior of graphene sheets based on nonlocal elasticity theory, *Steel and Composite Structures*, Vol. 30, No. 6, pp. 517-534, 2019.

[28] M. Shishesaz, M. Hosseini, K. N. Tahan, A. Hadi, Analysis of functionally graded nanodisks under thermoelastic loading based on the strain gradient theory, *Acta Mechanica*, Vol. 228, No. 12, pp. 4141-4168, 2017.

[29] A. Loghman, N. Shokouhi, Creep damage evaluation of thick-walled spheres using a long-term creep constitutive model, *Journal of Mechanical Science and Technology*, Vol. 23, No. 10, pp. 2577, 2009.

[30] D. Deepak, V. Gupta, A. Dham, Creep modeling in functionally graded rotating disc of variable thickness, *Journal of Mechanical science and Technology*, Vol. 24, No. 11, pp. 2221-2232, 2010.

[31] A. Loghman, A. G. Arani, A. Shajari, S. Amir, Time-dependent thermoelastic creep analysis of rotating disk made of Al–SiC composite, *Archive of Applied Mechanics*, Vol. 81, No. 12, pp. 1853-1864, 2011.

[32] H. Moon, K. M. Kim, Y. H. Jeon, S. Shin, J. S. Park, H. H. Cho, Effect of thermal stress on creep lifetime for a gas turbine combustion liner, *Engineering Failure Analysis*, Vol. 47, pp. 34-40, 2015.

[33] T. Bose, M. Rattan, Modeling creep behavior of thermally graded rotating disc of functionally graded material, *Differential Equations and Dynamical Systems*, pp. 1-14, 2017.

[34] A. Loghman, M. Moradi, Creep damage and life assessment of thick-walled spherical reactor using Larson–Miller parameter, *International Journal of Pressure Vessels and Piping*, Vol. 151, pp. 11-19, 2017.

[35] T. Bose, M. Rattan, Modeling creep analysis of thermally graded anisotropic rotating composite disc, *International Journal of Applied Mechanics*, Vol. 10, No. 06, pp. 1850063, 2018.

[36] M. Bahrampour, S. Hamzeh Javaran, S. Shojaee, New insight into viscoelastic finite element modeling of time-dependent material creep problems using spherical Hankel element framework, *International Journal of Applied Mechanics*, Vol. 10, No. 08, pp. 1850085, 2018.

[37] H. Mohammadi Hooyeh, A. Loghman, Creep damage and remnant life prediction of rotating hollow shaft based on the design strain and theta projection concept, *Mechanics of Advanced Materials and Structures*, Vol. 26, No. 11, pp. 967-974, 2019.

[38] R. K. Desu, H. N. Krishnamurthy, A. Balu, A. K. Gupta, S. K. Singh, Mechanical properties of Austenitic Stainless Steel 304L and 316L at elevated temperatures, *Journal of Materials Research and Technology*, Vol. 5, No. 1, pp. 13-20, 2016.

[39] A. Ghorbanpour Arani, R. Kolahchi, A. Mosallaie Barzoki, A. Loghman, Time-dependent thermo-electro-mechanical creep behavior of radially polarized FGPM rotating cylinder, *Journal of Solid Mechanics*, Vol. 3, No. 2, pp. 142-157, 2011.

[40] H.-L. Dai, H.-J. Jiang, L. Yang, Time-dependent behaviors of a FGPM hollow sphere under the coupling of multi-fields, *Solid State Sciences*, Vol. 14, No. 5, pp. 587-597, 2012.

[41] S. H. Kordkheili, M. Livani, Thermoelastic creep analysis of a functionally graded various thickness rotating disk with temperature-dependent material properties, *International Journal of Pressure Vessels and Piping*, Vol. 111, pp. 63-74, 2013.

[42] M. Davoudi Kashkoli, M. Zamani Nejad, Effect of heat flux on creep stresses of thick-walled cylindrical pressure vessels, *Journal of applied research and technology*, Vol. 12, No. 3, pp. 585-597, 2014.

[43] M. D. Kashkoli, M. Z. Nejad, Time-dependent thermo-elastic creep analysis of thick-walled spherical pressure vessels made of functionally graded materials, *Journal of Theoretical and Applied Mechanics*, Vol. 53, 2015.

[44] H. Zharfi, H. EkhteraeiToussi, Time dependent creep analysis in thick FGM rotating disk with two-dimensional pattern of heterogeneity, *International Journal of Mechanical Sciences*, Vol. 140, pp. 351-360, 2018.

[45] Y. Yang, Time-dependent stress analysis in functionally graded materials, *International Journal of Solids and Structures*, Vol. 37, No. 51, pp. 7593-7608, 2000.

[46] L. You, H. Ou, Z. Zheng, Creep deformations and stresses in thick-walled cylindrical vessels of functionally graded materials subjected to internal pressure, *Composite Structures*, Vol. 78, No. 2, pp. 285-291, 2007.

[47] A. Loghman, A. G. Arani, S. Amir, A. Vajedi, Magnetothermoelastic creep analysis of functionally graded cylinders, *International Journal of Pressure Vessels and Piping*, Vol. 87, No. 7, pp. 389-395, 2010.

[48] T. Singh, V. Gupta, Steady-state creep analysis of a functionally graded thick cylinder subjected to internal pressure and thermal gradient, *International journal of materials research*, Vol. 103, No. 8, pp. 1042-1051, 2012.
[49] T. Singh, V. Gupta, Analysis of steady state creep in whisker reinforced functionally graded thick cylinder subjected to internal pressure by considering residual stress, *Mechanics of Advanced Materials and Structures*, Vol. 21, No. 5, pp. 384-392, 2014.
[50] M. Nejad, Z. Hoseini, A. Niknejad, M. Ghannad, Steady-state creep deformations and stresses in FGM rotating thick cylindrical pressure vessels, *Journal of Mechanics*, Vol. 31, No. 1, pp. 1-6, 2015.
[51] M. Arefi, M. Nasr, A. Loghman, Creep analysis of the FG cylinders: Time-dependent non-axisymmetric behavior, *Steel and Composite Structures*, Vol. 28, No. 3, pp. 331-347, 2018.
[52] M. Moradi, A. Loghman, Non-Axisymmetric Time-Dependent Creep Analysis in a Thick-Walled Cylinder Due to the Thermo-mechanical loading, *Journal of Solid Mechanics*, Vol. 10, No. 4, pp. 845-863, 2018.
[53] M. Ghannad, M. Z. Nejad, Elastic analysis of pressurized thick hollow cylindrical shells with clamped-clamped ends, *Mechanics*, Vol. 85, No. 5, pp. 11-18, 2010.
[54] M. Ghannad, M. Z. Nejad, G. Rahimi, H. Sabouri, Elastic analysis of pressurized thick truncated conical shells made of functionally graded materials, *Structural Engineering and Mechanics*, Vol. 43, No. 1, pp. 105-126, 2012.
[55] M. Ghannad, G. H. Rahimi, M. Z. Nejad, Determination of displacements and stresses in pressurized thick cylindrical shells with variable thickness using perturbation technique, *Mechanics*, Vol. 18, No. 1, pp. 14-21, 2012.
[56] M. Ghannad, M. Z. Nejad, Elastic analysis of heterogeneous thick cylinders subjected to internal or external pressure using shear deformation theory, *Acta Polytechnica Hungarica*, Vol. 9, No. 6, pp. 117-136, 2012.
[57] M. Ghannad, M. Z. Nejad, Elastic solution of pressurized clamped-clamped thick cylindrical shells made of functionally graded materials, *Journal of theoretical and applied mechanics*, Vol. 51, No. 4, pp. 1067-1079, 2013.
[58] M. Ghannad, G. H. Rahimi, M. Z. Nejad, Elastic analysis of pressurized thick cylindrical shells with variable thickness made of functionally graded materials, *Composites Part B: Engineering*, Vol. 45, No. 1, pp. 388-396, 2013.
[59] M. Z. Nejad, M. Jabbari, M. Ghannad, Elastic analysis of FGM rotating thick truncated conical shells with axially-varying properties under non-uniform pressure loading, *Composite Structures*, Vol. 122, pp. 561-569, 2015.
[60] M. Zakeri, R. Attarnejad, Numerical free vibration analysis of higher-order shear deformable beams resting on two-parameter elastic foundation, *Journal of Computational Applied Mechanics*, Vol. 46, No. 2, pp. 117-131, 2015.
[61] H. Raissi, M. Shishesaz, S. Moradi, Applications of higher order shear deformation theories on stress distribution in a five layer sandwich plate, *Journal of Computational Applied Mechanics*, Vol. 48, No. 2, pp. 233-252, 2017.
[62] A. Zargaripoor, A. Bahrami, M. Nikkhah Bahrami, Free vibration and buckling analysis of third-order shear deformation plate theory using exact wave propagation approach, *Journal of Computational Applied Mechanics*, Vol. 49, No. 1, pp. 102-124, 2018.
[63] R. Javidi, M. Moghimi Zand, K. Dastani, Dynamics of Nonlinear rectangular plates subjected to an orbiting mass based on shear deformation plate theory, *Journal of Computational Applied Mechanics*, Vol. 49, No. 1, pp. 27-36, 2018.
[64] H. Matsunaga, Free vibration and stability of functionally graded circular cylindrical shells according to a 2D higher-order deformation theory, *Composite Structures*, Vol. 88, No. 4, pp. 519-531, 2009.
[65] H.-T. Thai, S.-E. Kim, A review of theories for the modeling and analysis of functionally graded plates and shells, *Composite Structures*, Vol. 128, pp. 70-86, 2015.
[66] M. Ghannad, M. Z. Nejad, G. Rahimi, Elastic solution of axisymmetric thick truncated conical shells based on first-order shear deformation theory, *Mechanics*, Vol. 79, No. 5, pp. 13-20, 2009.
[67] M. Ghannad, M. Jabbari, M. Nejad, An elastic analysis for thick cylindrical pressure vessels with variable thickness, *Engineering Solid Mechanics*, Vol. 3, No. 2, pp. 117-130, 2015.
[68] M. Jabbari, M. Z. Nejad, M. Ghannad, Thermo-elastic analysis of axially functionally graded rotating thick cylindrical pressure vessels with variable thickness under mechanical loading, *International journal of engineering science*, Vol. 96, pp. 1-18, 2015.
[69] M. Jabbari, M. Z. Nejad, M. Ghannad, Thermo-elastic analysis of axially functionally graded rotating thick truncated conical shells with varying thickness, *Composites Part B: Engineering*, Vol. 96, pp. 20-34, 2016.

[70] M. Z. Nejad, M. Jabbari, M. Ghannad, Elastic analysis of rotating thick cylindrical pressure vessels under non-uniform pressure: linear and non-linear thickness, *Periodica Polytechnica Mechanical Engineering*, Vol. 59, No. 2, pp. 65-73, 2015.

[71] A. Sofiyev, Application of the first order shear deformation theory to the solution of free vibration problem for laminated conical shells, *Composite Structures*, Vol. 188, pp. 340-346, 2018.

[72] H. Gharooni, M. Ghannad, Nonlinear analysis of radially functionally graded hyperelastic cylindrical shells with axially-varying thickness and non-uniform pressure loads based on perturbation theory, *Journal of Computational Applied Mechanics*, Vol. 50, No. 2, pp. 324-340, 2019.

[73] H. Gharooni, M. Ghannad, Nonlinear analytical solution of nearly incompressible hyperelastic cylinder with variable thickness under non-uniform pressure by perturbation technique, *Journal of Computational Applied Mechanics*, Vol. 50, No. 2, pp. 395-412, 2019.

[74] H. R. Eipakchi, Third-order shear deformation theory for stress analysis of a thick conical shell under pressure, *Journal of Mechanics of materials and structures*, Vol. 5, No. 1, pp. 1-17, 2010.

[75] M. Ghannad, H. Gharooni, Elastic analysis of pressurized thick FGM cylinders with exponential variation of material properties using TSDT, *Latin American journal of solids and structures*, Vol. 12, No. 6, pp. 1024-1041, 2015.

[76] H. Gharooni, M. Ghannad, M. Z. Nejad, Thermo-elastic analysis of clamped-clamped thick FGM cylinders by using third-order shear deformation theory, *Latin American Journal of Solids and Structures*, Vol. 13, No. 4, pp. 750-774, 2016.

[77] M. Jabbari, M. Zamani Nejad, M. Ghannad, Stress analysis of rotating thick truncated conical shells with variable thickness under mechanical and thermal loads, *Journal of Solid Mechanics*, Vol. 9, No. 1, pp. 100-114, 2017.

[78] M. Kashkoli, K. N. Tahan, M. Nejad, Time-dependent creep analysis for life assessment of cylindrical vessels using first order shear deformation theory, *Journal of Mechanics*, Vol. 33, No. 4, pp. 461, 2017.

[79] M. D. Kashkoli, M. Z. Nejad, Time-dependent creep analysis and life assessment of 304 L austenitic stainless steel thick pressurized truncated conical shells, *Steel and Composite Structures*, Vol. 28, No. 3, pp. 349-362, 2018.

[80] M. D. Kashkoli, K. N. Tahan, M. Z. Nejad, Time-dependent thermomechanical creep behavior of FGM thick hollow cylindrical shells under non-uniform internal pressure, *International Journal of Applied Mechanics*, Vol. 9, No. 06, pp. 1750086, 2017.

[81] M. D. Kashkoli, K. N. Tahan, M. Z. Nejad, Thermomechanical creep analysis of FGM thick cylindrical pressure vessels with variable thickness, *International Journal of Applied Mechanics*, Vol. 10, No. 01, pp. 1850008, 2018.

[82] J. Jelwan, M. Chowdhry, G. Pearce, Creep life forecasting of weldment, 2011.

[83] E. L. Robinson, Effect of temperature variation on the long-time rupture strength of steels, *Trans. ASME*, Vol. 77, 1952.

[84] R. Ainsworth, P. Budden, Design and assessment of components subjected to creep, *The Journal of Strain Analysis for Engineering Design*, Vol. 29, No. 3, pp. 201-207, 1994.

[85] J. Kropiwnicki, M. Hack, Improved calculation of damage due creep by more accurate time to rupture data representation, 2006.

[86] M. Sabour, R. Bhat, Lifetime prediction in creep-fatigue environment, *Materials Science-Poland*, Vol. 26, No. 3, pp. 563-584, 2008.

[87] F. V. Tahami, A. H. Daei-Sorkhabi, F. R. Biglari, Creep constitutive equations for cold-drawn 304L stainless steel, *Materials Science and Engineering: A*, Vol. 527, No. 18-19, pp. 4993-4999, 2010.